Applied Surface Science 384 (2016) 182–191

Contents lists available at ScienceDirect

Applied Surface Science

journal homepage: www.elsevier.com/locate/apsusc

Two-step flash light sintering of copper nanoparticle ink to remove substrate warping

Chung-Hyeon Ryu [a], Sung-Jun Joo [a], Hak-Sung Kim [a,b,*]

[a] Department of Mechanical Convergence Engineering, Hanyang University, Haengdang-dong, Seongdong-gu, Seoul 133-791, South Korea
[b] Institute of Nano Science and Technology, Hanyang University, Seoul, 133-791, South Korea

ARTICLE INFO

Article history:
Received 23 November 2015
Received in revised form 20 April 2016
Accepted 4 May 2016
Available online 6 May 2016

Keywords:
Printed electronics
Two-step flash light sintering
Substrate warping
In situ monitoring
copper nanoparticles

ABSTRACT

A two-step flash light sintering process was devised to reduce the warping of polymer substrates during the sintering of copper nanoparticle ink. To determine the optimum sintering conditions of the copper nanoparticle ink, the flash light irradiation conditions (pulse power, pulse number, on-time, and off-time) were varied and optimized. In order to monitor the flash light sintering process, in situ resistance and temperature monitoring of copper nanoink were conducted during the flash light sintering process. Also, a transient heat transfer analysis was performed by using the finite-element program ABAQUS to predict the temperature changes of copper nanoink and polymer substrate. The microstructures of the sintered copper nanoink films were analyzed by scanning electron microscopy. Additionally, an X-ray diffraction and Fourier transform infrared spectroscopy were used to characterize the crystal phase change of the sintered copper nanoparticles. The resulting two-step flash light sintered copper nanoink films exhibited a low resistivity (3.81 μΩ cm, 2.3 times of that of bulk copper) and 5B level of adhesion strength without warping of the polymer substrate.

1. Introduction

Recently, the flexible printed circuit board (FPCB) market has expanded as the use of smart devices, such as smart phones and tablet PCs, have gradually increased. FPCBs have been fabricated by photolithography processes. However, conventional photolithography has a high cost and is a time-consuming process because it has several process steps, such as exposure, developing, and etching [1]. For these reasons, the printing of electronics, which is a convenient and low-cost process, has been adopted as an advanced alternative [2–5].

Printed electronics on polymer substrates have various applications such as flexible displays, flexible solar cells, wearable electronics, organic light emitting diodes, radio frequency identification tags, and flexible touch pads [6–9]. The key component of printed electronics is the fabrication of conductive circuits. For conductive circuits, metal nanoparticle pastes, such as silver and gold, have been used because of their low melting point and oxidation stabilities [10–12]. However, silver and gold are too expensive for commercialization. For this reason, copper nanopastes have been developed as an alternative to silver and gold. However, most copper nanoparticles are easily oxidized or already covered with oxide shells [13]. Therefore, the flash light sintering process combined with poly(*N*-vinylpyrrolidone) (PVP) functionalization of copper nanoparticles was proposed to overcome this problem [14–17]. The flash light sintering method can immediately remove the oxide shells of copper nanoparticles and form pure copper films at room temperature in ambient conditions [16]. In our previous papers, we optimized the one-step flash light irradiation condition for sintering copper nanopastes on a polyimide (PI) substrate with a 225 μm thickness [14]. In the previous work, the copper nanopastes were fully sintered without any damage to the PI substrates. However, for thinner substrates, the flexible substrates were bent and easily damaged during the flash light sintering. These phenomena have been considered a critical problem to the reliability and productivity of electronic devices.

Therefore, in this study, a two-step flash light sintering method was employed to reduce substrate warping and enhance the electrical conductivity compared to the conventional one-step flash light sintering method (Fig. 1). In order to monitor the real time sintering process, in situ monitoring of the resistance and temperature of copper nanoink were performed using a Wheatstone bridge circuit and thermocouple based circuit, respectively. A heat transient transfer analysis was conducted by using ABAQUS to calculate temperature field of copper nanoink film and PI substrate during one-

* Corresponding author at: Department of Mechanical Convergence Engineering, Hanyang University, Haengdang-dong, Seongdong-gu, Seoul 133–791, South Korea.
E-mail address: kima@hanyang.ac.kr (H.-S. Kim).

http://dx.doi.org/10.1016/j.apsusc.2016.05.025
0169-4332/

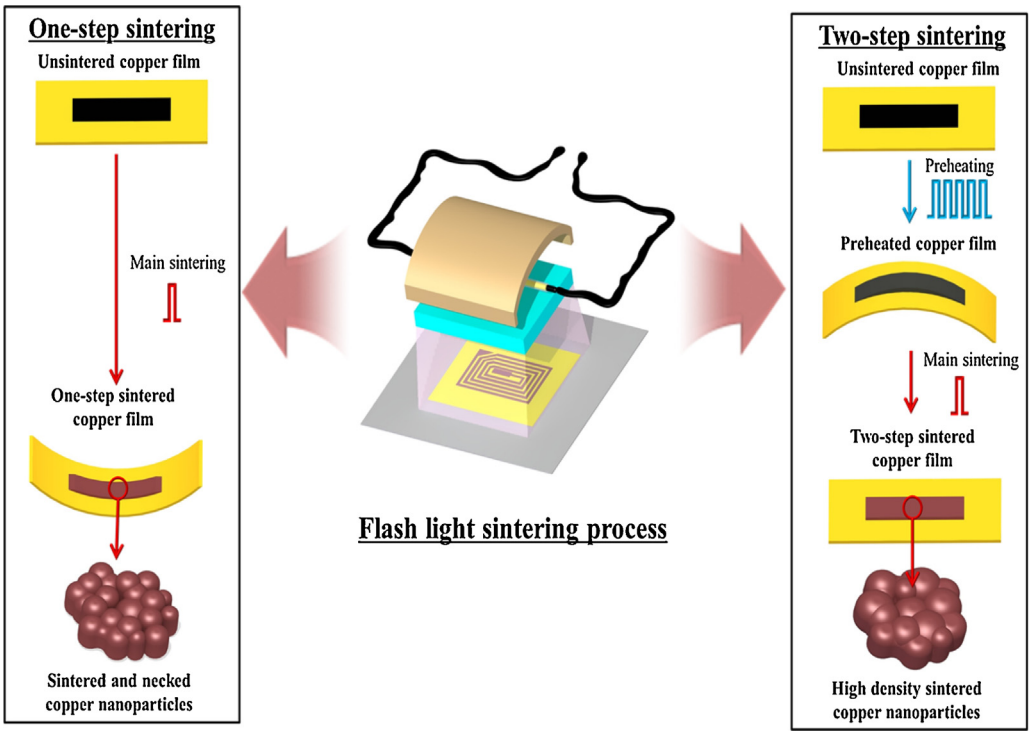

Fig. 1. Schematic diagram of one- and two-step flash light sintering processes.

and two-step flash light sintering processes. The sintered copper nanoink films were characterized using several microscopic and spectroscopic techniques, including scanning electron microscopy (SEM), X-ray diffraction (XRD) and Fourier transform infrared spectroscopy (FT-IR).

2. Material and methods

2.1. Specimen preparation

To prepare the conductive copper nanoink films, copper nanoparticles with oxide shells (mean particle size: 40 nm, oxide shell thickness >2 nm, Quantum Sphere Inc.) were used [17]. First, 0.9 g of PVP (MW 55,000, Sigma Aldrich Co.) was dissolved in 3.0 g of diethylene glycol (DEG, Sigma Aldrich Co.). After that, 11.4 g of copper nanoparticles were dispersed in this mixed solvent with 3-roll milling for 30 min. The fabricated copper nanoinks (solid contents: 80%) were printed on PI substrates (PI, SKC KOLON) with a 50 μm thickness using a screen printer (Tiger SP2825-MT, Daeyoung High Tech Co., printing speed: 100 mm/s). The printed copper nanoink films were then dried using near infrared (NIR, wavelength range: 800–1500 nm, 500 W; Adphos L40) for 10 min at 100 °C.

2.2. Two-step flash light sintering

Flash light irradiation was used for the sintering of the printed copper nanoink films. This process was performed at room temperature in ambient conditions. The flash light sintering system is composed of a xenon lamp (PerkinElmer Co.), a simmer triggering pulse controller, a power supply, capacitors, and a water cooling system [14,15]. In this system, the xenon lamp generated white light over a wide range of wavelengths (from 380 to 950 nm). In this study, the flash light was applied at two steps; preheating sintering and main sintering. The preheating step was performed to reduce the substrate warping and decompose some of the organic binder in the copper nanoink films. In the preheating step, the flash light irradiation energy was varied from 6 to 12 J/cm^2, while the other flash light irradiation conditions, including the number of pulses (35), on-time (1 ms), and off-time (30 ms), were fixed. After the preheating step, the main sintering step was performed to sinter the copper nanoink films. The flash light irradiation energy was varied from 3 to 9 J/cm^2 with 3 ms on-time and single pulses. The energy of the irradiated flash light was measured by a power meter (Nove II, People Laser Tech.).

Table 1
Material constants of copper, PI, and aluminum.

	Copper	PI	Aluminum
Thermal conductivity (k, W/m °C)	401	0.52	170
Specific gravity (ρ, J/kg °C)	8940	1430	2700
Specific heat capacity (C_p, J/kg °C)	384.6	1150	950
Melting temperature (T_m, °C)	250[a]	–	–
Latent heat of fusion (H, J/kg)	2.05×10^5	–	–

[a] Mean-size of copper nanoparticles: 40 nm.

2.3. Transient heat transfer analysis

The commercial finite element software package ABAQUS 6.12 (Hibbitt, Karlsson and Sorensen, USA) was employed to perform transient heat transfer analysis about copper nanoink film and PI substrate. Fig. 2 shows the finite element model and mesh structure, the x- and y-dimensions are each 1 cm, and the thickness of each component (copper, PI film, and aluminum plate) is based on the real-size of specimen (Table 1). In this model, the 10 μm thick of copper nanoink film was positioned on the 50 μm thick of PI substrate. Also, aluminum plate which has 5 mm thickness was placed as floor beneath of the PI film. This model neglected the effect of PVP due to small amount and minimal influence of it [18]. The interfaces between each layer were perfectly attached by using the *TIE function in ABAQUS. The initial temperature of model is regarded as room temperature, 20 °C. In order to simulate the flash light irradiation, it is assumed that the irradiation energy is converted into

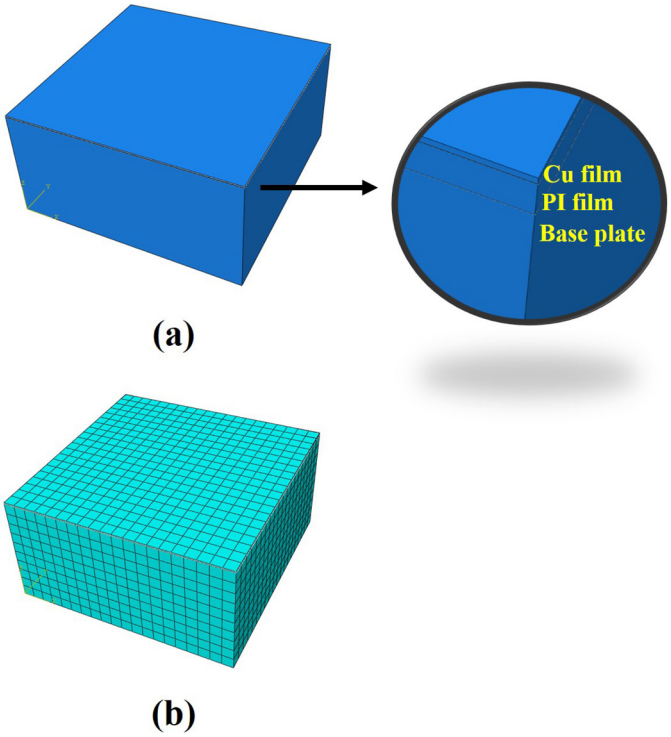

Fig. 2. (a) The finite element model and (b) meshed structure of copper nanoink film on PI substrates.

heat instantly. Since the flash light irradiates the top of the copper film, the surface heat flux was generated on the top of the copper film. The heat transfer equation of flash light irradiation energy into the film and substrates is described as:

$$\rho c_P \frac{\partial T}{\partial t} = \nabla \cdot (k \nabla T) + Q \quad (1)$$

where T is temperature, p is density, c_p is specific heat capacity, k is thermal conductivity, and Q is internal heat generation. These above material constants were employed from Ref. [19]. For the base plate which was made with aluminum, the material property was received by manufacturer. Boundary conditions of surfaces exposed by air are described as

$$k \frac{\Delta T}{\Delta n} = -h(T_s - T_\infty) \quad (2)$$

where n is normal vector to the surface, h is the convection coefficient of the surface, T_s is the surface temperature, and T_∞ is the atmosphere temperature. For a surface condition, the convection coefficient h is considered natural convection of 30 W/m^2K because there is no additional cooling system. The effect of radiation heat was neglected in this model [19]. From this analysis, the temperature changes of copper nanoink film and PI substrates in respect to time and depth were investigated during one- and two-step flash light sintering processes.

2.4. Characterization

To measure the electrical resistivity of the copper nanoink films, the electrical sheet resistance and the thickness of the sintered copper nanoink films were measured using a four-point probe method and an alpha step (KLA Tencor AS500, Tencor instruments), respectively. The adhesion strength of sintered copper nanoink films were assessed with the 3 M tape test (ASTM D3359) [20]. The in situ monitoring system was used to measure the resistance and temperature changes in real time during the flash light sintering process. This

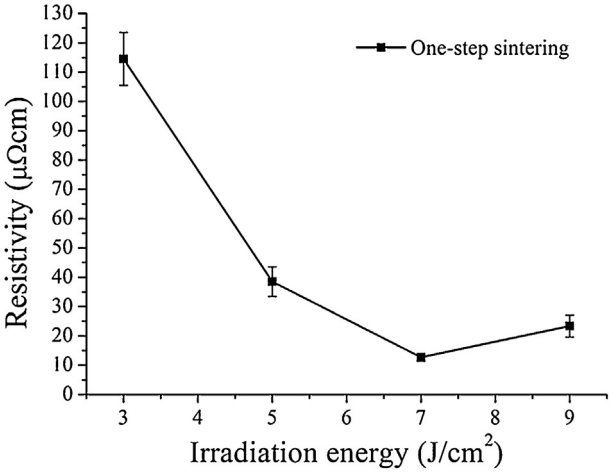

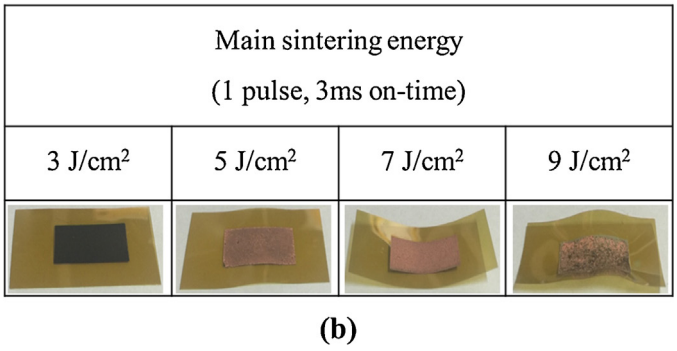

Fig. 3. (a) The resistivity and (b) optical images of one-step sintered copper nanoparticles ink with respect to the main sintering energy.

in situ resistance monitoring system was composed of a Wheatstone bridge circuit, oscilloscope, and source meter. Additionally, an in situ temperature monitoring system was devised with a non-inverting amplifier circuit with an op-amp (LM 324N, STMicroelectronics), a power supply (SDP 30-3DT, SM Techno), and type-K thermocouple (Labfa-cility, UK). To determine the glass transition temperature of the PI film, differential scanning calorimetry (DSC; SDT-Q600, TA instruments) was performed (measuring condition: 5 °C/min in N_2 gas condition). The microstructure of the copper nanoparticles was observed via an SEM (S4800, Hitachi, 15 kV operating voltage). To characterize the phases of the materials, crystal phase analysis was conducted using XRD (D/MAX 2500, Rigaku) and FT-IR (Bruker IFS-66/s, Bruker Co.).

3. Results and discussion

For the sintering of copper nanoink films, the irradiation energy was varied from 3 to 9 J/cm^2 with the other fixed variables in the flash light conditions (on-time: 3 ms and single pulse). Fig. 3 shows the resistivity and optical image of the one-step sintered copper nanoink films. As shown in Fig. 3(a), the resistivity of the copper nanoink films decreased as the irradiation energy was increased. When the irradiation energy was 9 J/cm^2, the copper nanoink films were partially burned (Fig. 3(b)). In this case, the resistivity of the copper nanoink films increased slightly compared to that of the 7 J/cm^2 irradiated copper nanoink films. Therefore, the 7 J/cm^2 irradiation energy was chosen as the optimum energy. For the 7 J/cm^2 irradiation energy, the resistivity of the copper nanoink film was 12.68 μΩ cm, which is greater than that of the bulk copper

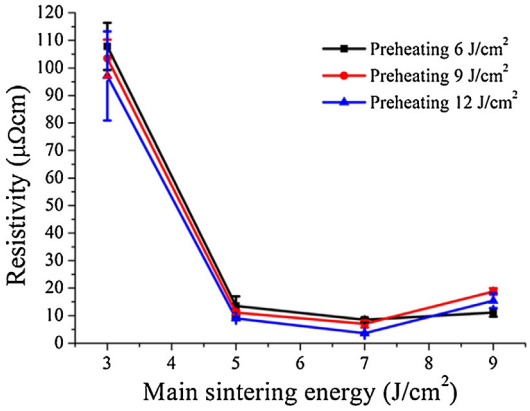

(a)

		Main sintering energy (1 pulse, 3ms on-time)			
		3 J/cm²	5 J/cm²	7 J/cm²	9 J/cm²
Preheating Energy (35 pulse, 1 ms on-time, 30 ms off-time)	6 J/cm²	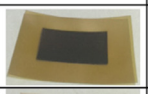		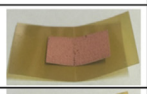	
	9 J/cm²		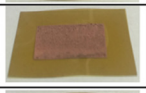	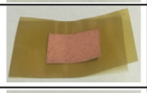	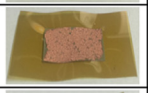
	12 J/cm²		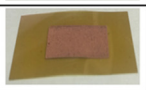	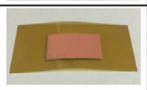	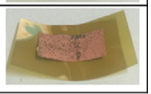

(b)

Fig. 4. (a) The resistivity and (b) optical images of two-step sintered copper nanoparticles ink with respect to the preheating energy and main sintering energy.

(1.68 μΩ cm). Additionally, as shown in Fig. 3(b), the PI substrates bent when the copper nanoink was fully sintered.

The two-step flash light sintering method was performed in order to reduce the substrate warping. Fig. 4 shows the resistivity and optical image of the two-step sintered copper nanoink films with respect to the preheating and main sintering conditions. In the preheating process, the total flash light irradiation energy was varied from 6 to 12 J/cm^2 (on-time: 1 ms, off-time: 30 ms, pulse number: 35). After preheating, the single flash light application for the main sintering was applied for 3 ms of on-time, varying the light energy from 3 to 9 J/cm^2. As shown in Fig. 4(a), the resistivity of the sintered copper nanoink films decreased as the irradiation energy increased. When the main sintering energy was 3 J/cm^2, the copper nanoink film was not fully sintered, regardless of the preheating energy, because of the insufficient light energy. When the main sintering energy was 9 J/cm^2, the copper nanoink film was bent and partially damaged because of excessive irradiation energy. Accordingly, the 7 J/cm^2 main sintering energy was the optimum power for the main sintering of copper nanoparticles. Based on these results, the resistivity of the copper nanoink film was measured as 3.81 μΩ cm, 0.3 times of that of the one-step sintered copper nanoink film. As shown in Fig. 4(b), the PI substrate warping was remarkably reduced compared to the one-step flash light sintered copper nanoink film (see Fig. 3(b)).

Fig. 5 shows the adhesion test results of the one-step (7 J/cm^2 main sintering) and two-step (12 J/cm^2 preheating and 7 J/cm^2 main sintering) sintered copper nanoink films. As shown in Fig. 5(a), some of the copper patterns were peeled out when the one-step flash light energy was irradiated. Meanwhile, in the two-step flash light sintering case, the copper pattern did not be peeled out and it had 5B adhesion level (Fig. 5(b)). It might be because the high density of copper structure contributed to the high level of adhesion during the two-step sintering.

In order to analyze morphology of copper about various sintering conditions, SEM images of the copper nanoink film surface were obtained to. Fig. 6(a) shows the SEM images of the unsintered copper nanoink film. In the unsintered copper nanoink film, the PVP covered the copper nanoparticles well. After 6 J/cm^2 of preheating energy was applied, the PVP on the copper nanoparticles were slightly removed because the PVP decomposed during the preheating step (Fig. 6(b)). As the preheating energy was increased, more PVP was removed (Fig. 6(c) and (d)). Nevertheless, after the preheating process, necking among the copper nanoparticles was not observed. Fig. 7 shows the resistivity changes of the copper nanoink films measured using the in situ resistance monitoring system. As shown in Fig. 7, the resistivity remained infinite during the preheating process, regardless of the preheating energy, because the copper nanoparticles were not sintered and necked and only PVP was slightly removed (Fig. 6(b)–(d)). After the main sintering energy was irradiated, the resistivity of the preheated copper nanoink films drastically decreased to 8.45, 6.98, and 3.81 μΩ cm, respectively (Fig. 7(b)–(d)). All the cases were sintered well without re-oxidation phenomenon. Fig. 6(e) shows the SEM images of the one-step sintered copper nanoink film. In this case, necking between each copper nanoparticle was observed instead of an enlarged grainy structure. In the 6 J/cm^2 pre-

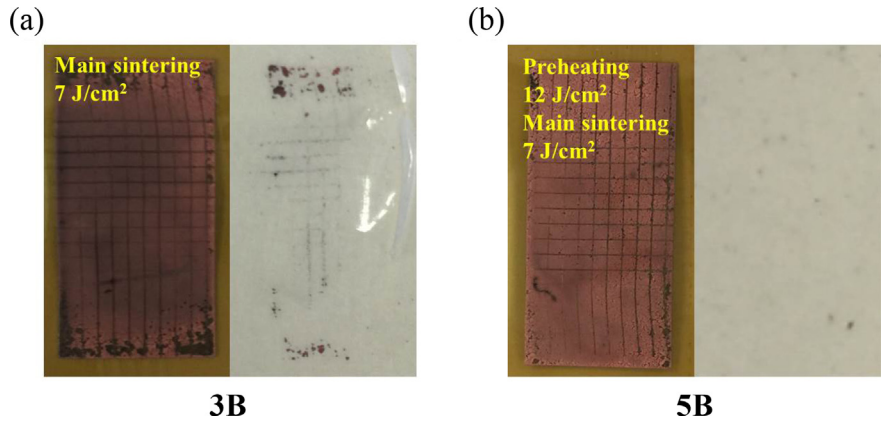

Fig. 5. Adhesion strength of sintered copper nanoink films after sintering: (a) one-step sintering and (b) two-step sintering methods.

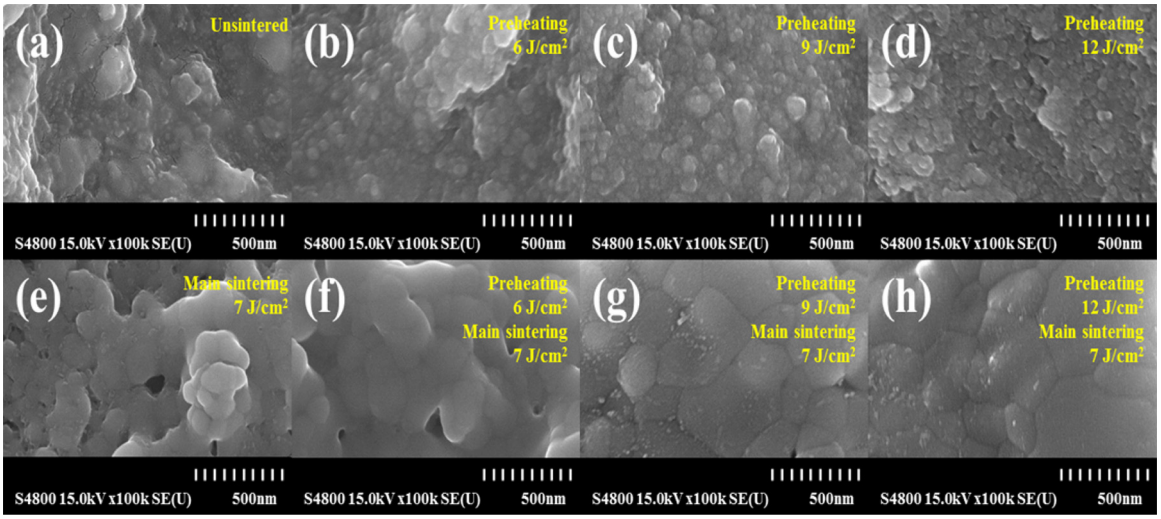

Fig. 6. SEM images of copper nanoparticles ink: (a) unsintered, (b) 6 J/cm^2 preheated, (c) 9 J/cm^2 preheated, (d) 12 J/cm^2 preheated, (e) 7 J/cm^2 main sintered, (f) 6 J/cm^2 preheated and 7 J/cm^2 main sintered, (g) 9 J/cm^2 preheated and 7 J/cm^2 main sintered, and (h) 12 J/cm^2 preheated and 7 J/cm^2 main sintered cases.

heated and 7 J/cm^2 main sintered copper nanoink film, the copper nanoparticles formed as a grainy structure (Fig. 6(f)). As the preheating energy was increased, the copper nanoparticles were more agglomerated and formed a larger grainy structure than those of the one-step sintered case (Fig. 6(f)–(h)). In the case of 12 J/cm^2 preheating followed by 7 J/cm^2 main sintering, the copper nanoparticles were formed as the largest and most uniform grainy structure, possibly due to the higher preheating temperature increasing the density of the sintered structure (Fig. 6(h)) [21,22].

Fig. 8 shows the in situ temperature monitoring and heat transfer analysis results of copper nanoink film during one-step and two-step sintering. As shown in Fig. 8(a), the temperature of the one-step sintered copper nanoink film instantly increased to 280 °C, allowing for the complete decomposition of PVP and sintering of the copper nanoparticles [23]. After the flash light irradiation ended, the sintered copper nanoparticles cooled rapidly and transformed into a solid phase [19]. This phenomenon is also observed in finite element analysis results, the temperature of copper nanoink film was increased abruptly up to 290 °C during flash light irradiation. Then, the heated copper nanoink film was cooled to room temperature with similar rate of experimental one. Based on correction of these results, finite element analysis of temperature profile in respect to depth and time was performed. Fig. 9(a) shows the temperature profile of copper nanoink film in thickness direction during one-step sintering process. The temperature of copper nanoink was sufficiently increased even bottom of the film due to the high conductivity of copper. It indicates that copper nanoink film was sufficiently heated to the bottom of the copper nanoink film (see Fig. 9(a)). Therefore, reduction of copper oxide and sintering reaction between copper nanoparticles occurred simultaneously for all the parts. However, these reactions might interfere the sintering phenomena between copper nanoparticles, resulting in relatively higher resistivity than that of two-step sintered case. In the two-step sintering case (Fig. 8(b)), the temperature of the preheated copper nanoink film slightly increased to around 230 °C, which could decompose the PVP [19,24], not sinter the copper nanoparticles. This result corresponds with finite element analysis results, as shown in Fig. 8(b). The temperature of copper nanoink film was increased gradually up to 230 °C during preheating process and also even to the bottom of the copper nanoink film (see Fig. 9(b)). The uniform increase of temperature of copper nanoink film allows decomposition of PVP and elimination of the copper oxide. However, in the preheating process, the sheet resistance was not changed because temperature was not sufficiently high to sinter the copper nanoparticles (Fig. 6(b)–(d)). It is because the diameter of nanoparticles used in this work is varied 20 nm–50 nm which have the melting point around 250 °C [23]. When the main sintering energy was irradiated, as shown in Fig. 8(b), the temperature of the copper nanoink film drastically increased to 280 °C. Therefore, in this temperature, sintering

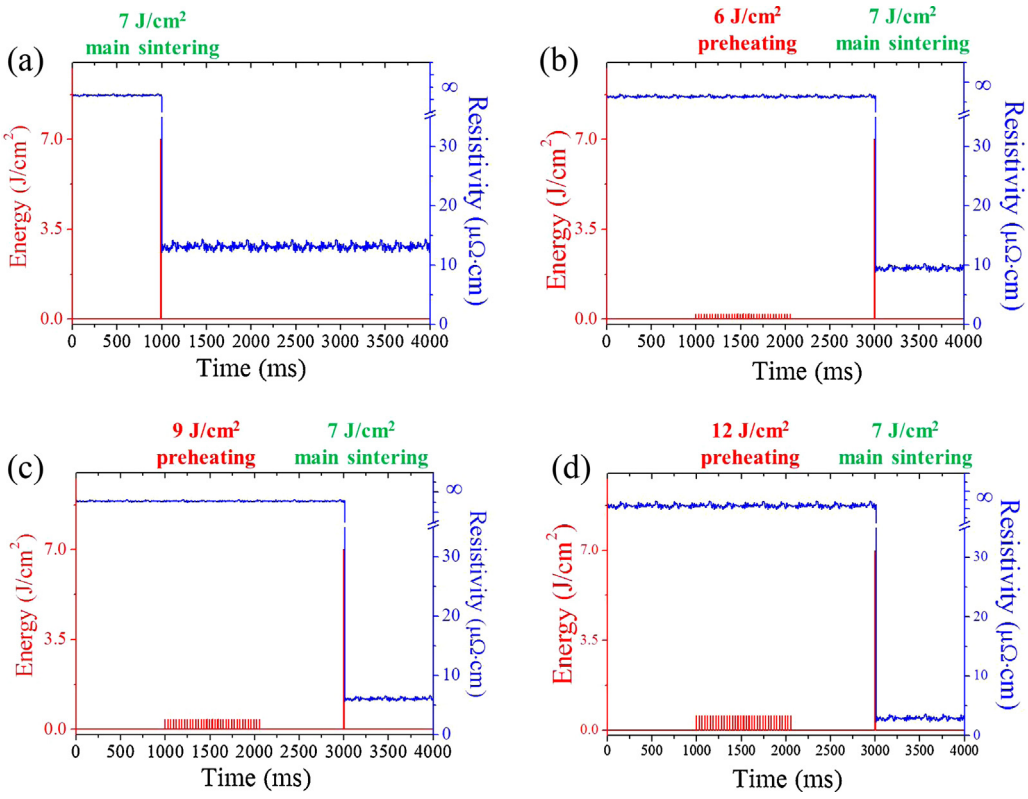

Fig. 7. In situ resistance monitoring results of copper nanoparticles ink during the flash light sintering process: (a) 7 J/cm^2 main sintered, (b) 6 J/cm^2 preheated and 7 J/cm^2 main sintered, (c) 9 J/cm^2 preheated and 7 J/cm^2 main sintered, and (d) 12 J/cm^2 preheated and 7 J/cm^2 main sintered.

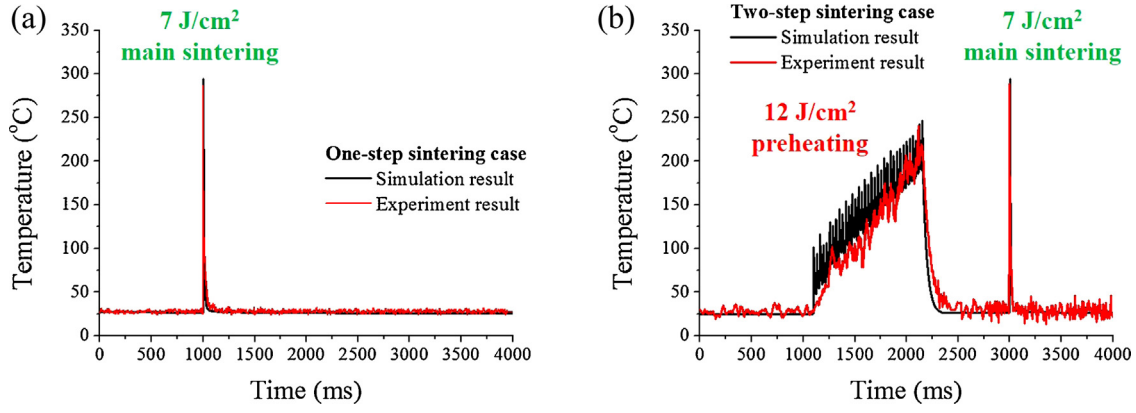

Fig. 8. In situ temperature monitoring and heat transfer analysis results of copper nanoparticles ink: (a) one-step sintered and (b) two-step sintered.

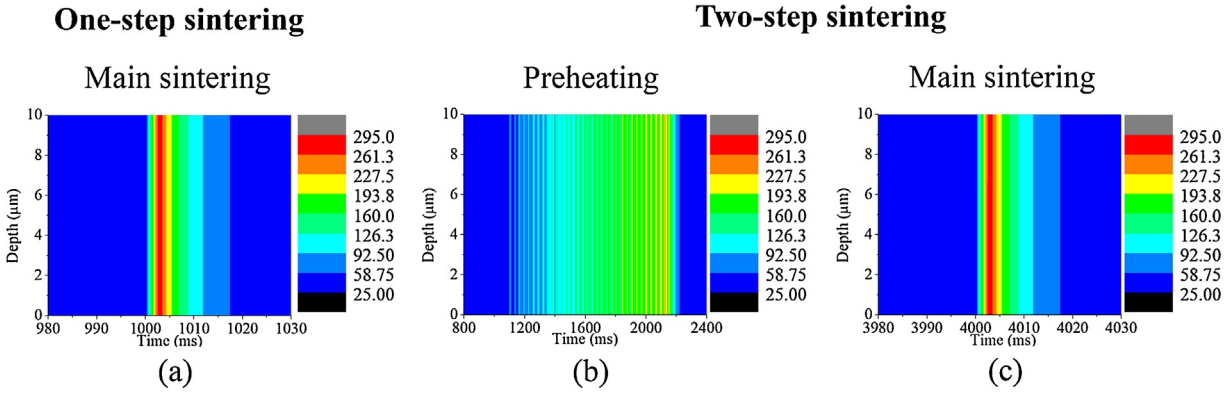

Fig. 9. The cross-sectional temperature profile of copper nanoink films: (a) main sintering process of one-step sintering, and (b) preheating and (c) main sintering of two-step sintering.

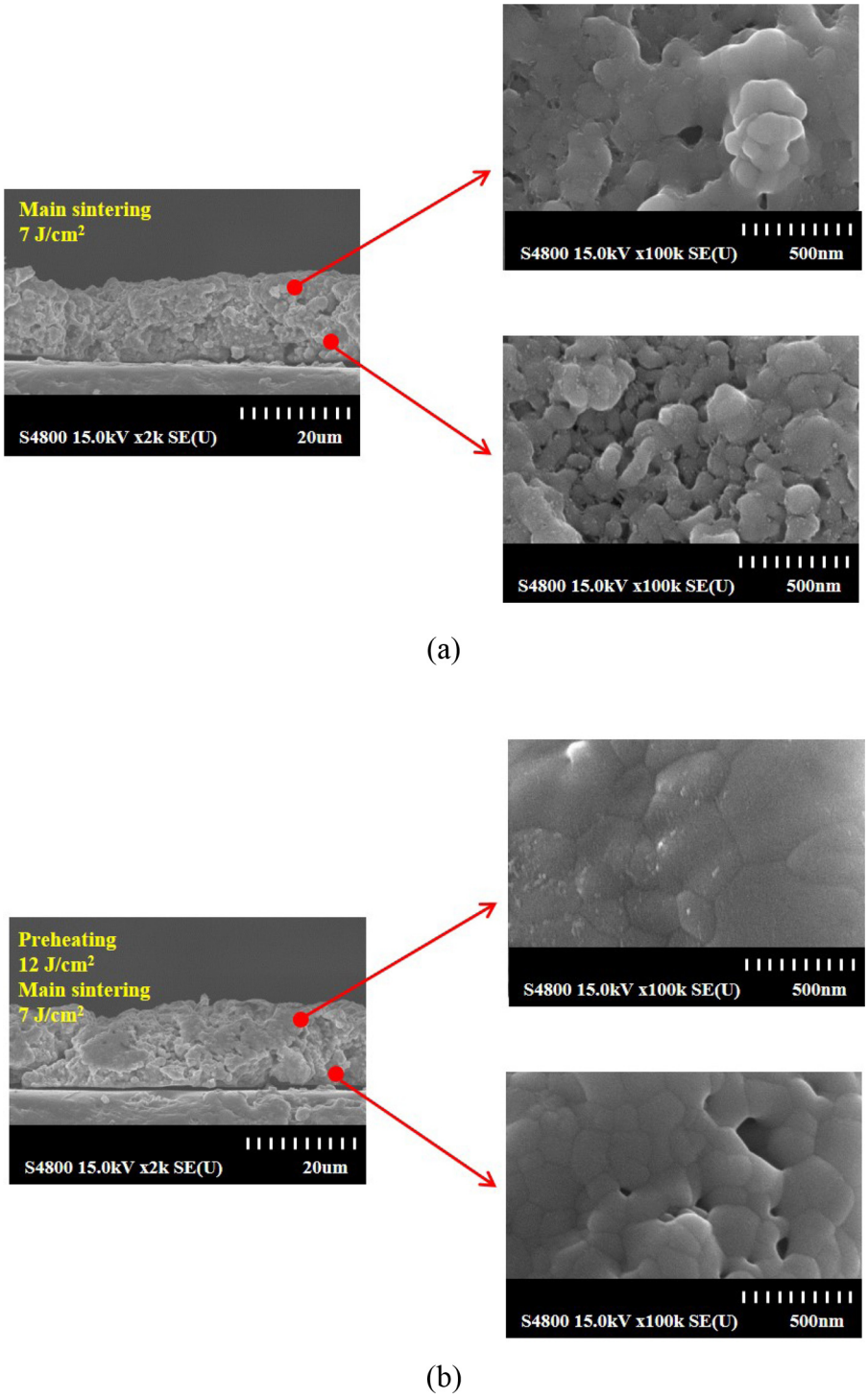

Fig. 10. The cross-sectional SEM images of copper nanoparticles ink: (a) one-step sintered and (b) two-step sintered.

phenomena and growth of grain boundary of copper nanoparticles occurred owing to the sufficient temperature for partially melting and sintering the copper nanoparticles (see Fig. 8(b) and 9(c)). Then, the heated copper nanoink film was decreased to room temperature, which is similar temperature trend with the one-step sintered copper nanoink film case. As a result, the two-step sintering method divides sintering process into two stages, reduction and sintering. By dividing the flash light sintering process, the high densification rate and grain growth was obtained after main-sintering process.

Fig. 10 shows the cross-sectional SEM images of the one-step (7 J/cm^2 main sintering) and two-step (12 J/cm^2 preheating and 7 J/cm^2 main sintering) sintered copper nanoink films. As shown in Fig. 10(a), in the one-step sintered copper nanoink film, the top side of the copper pattern was sintered and well necked, while the bottom side of the copper pattern was not. It is because simultaneous reactions such as oxide reduction and sintering of copper nanoparticles reduce the overall morphology quality of sintered copper structure, especially bottom of the copper nanoink film. On the other hand, the two-step sintered copper nanoink film case (see Fig. 10(b)) shows the well sintered and densely agglomerated on both the top and bottom sides of the copper pattern owing to the splitting oxide reduction and sintering pro-

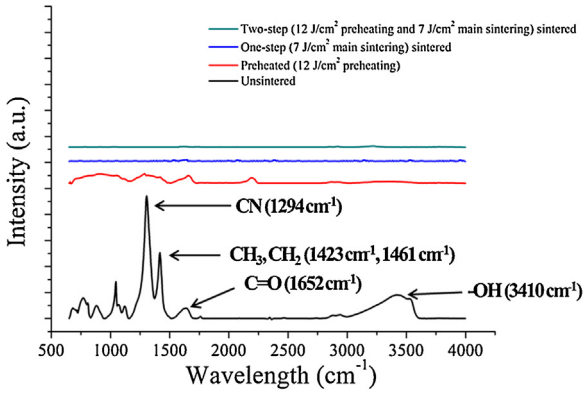

Fig. 11. The FT-IR spectra of copper nanoparticles ink with respect to the irradiation conditions.

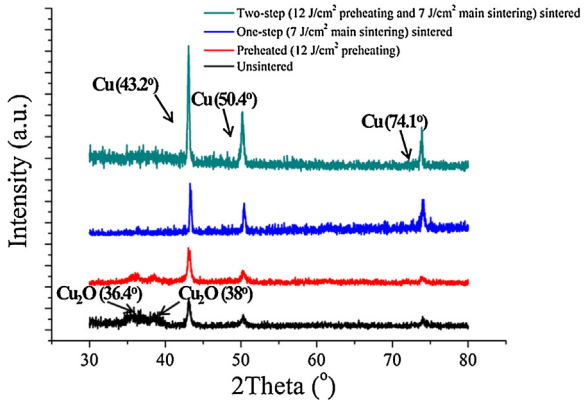

Fig. 12. The XRD patterns of copper nanoparticles ink with respect to the irradiation conditions.

cess, resulting in low resistivity and high adhesion strength (see Figs. 4 and 5).

To confirm the residual PVP after the flash light was applied, the FT-IR spectra of the copper nanoink films was analyzed (Fig. 11). The unsintered copper nanoink films showed many peaks, such as C—N (1294 cm^{-1}), CH_3 (1423 cm^{-1}), CH_2 (1461 cm^{-1}), C=O (1652 cm^{-1}) and –OH (3410 cm^{-1}), from the chemical bonding in PVP and copper nanoparticles. In the preheated copper nanoink films, the intensities of these peaks decreased significantly because some of the PVP were decomposed. This result was an evidence of our hypothesis that preheating decompose of PVP and eliminate the copper oxide (see explanation in Fig. 8). After the main sintering energy was applied, all peaks attributed to PVP disappeared completely [25–27]. Additionally, in the one-step sintered copper nanoink films case, most of the peaks disappeared.

Fig. 12 shows XRD of the sintered copper nanoink film. The XRD patterns of the unsintered copper nanoink films have pure copper peaks (43.2°, 50.4° and 74.1°) and oxidized copper peaks (36.4° and 38°). When 12 J/cm^2 preheating energy was applied, the intensity of the oxidized copper peak (36.4°) decreased and the pure copper peak (43.2°) slightly increased because the preheating energy reduced the PVP-functionalized copper oxide shells. However, the oxidized copper peaks still remained after the preheating process because the preheating energy was insufficient in evaporating all of the organic binder. The oxidized copper peaks (36.4° and 38°) disappeared and the intensities of the pure copper peaks increased after the 7 J/cm^2 main sintering energy was applied, due to the complete reduction of the copper oxide shells. Additionally, the two-step sintered copper nanoink film has a greater intensity of the pure copper peak than the one-step sintered copper nanoink film.

The optical image of the sintered copper nanoink film with optimum two-step flash light irradiation condition (12 J/cm^2 of preheating followed by the 7 J/cm^2 of main sintering) was shown in Fig. 13(a). The copper nanoink film was bent in a convex shape when the 12 J/cm^2 preheating energy was applied. Then, after irradiating with the 7 J/cm^2 main sintering energy, the copper nanoink film became flat again (Fig. 13(a)). Fig. 13(b) depicts the schematic diagram of the substrate warping reduction. Also, the shrinkage occurred during main-sintering process. During the preheating

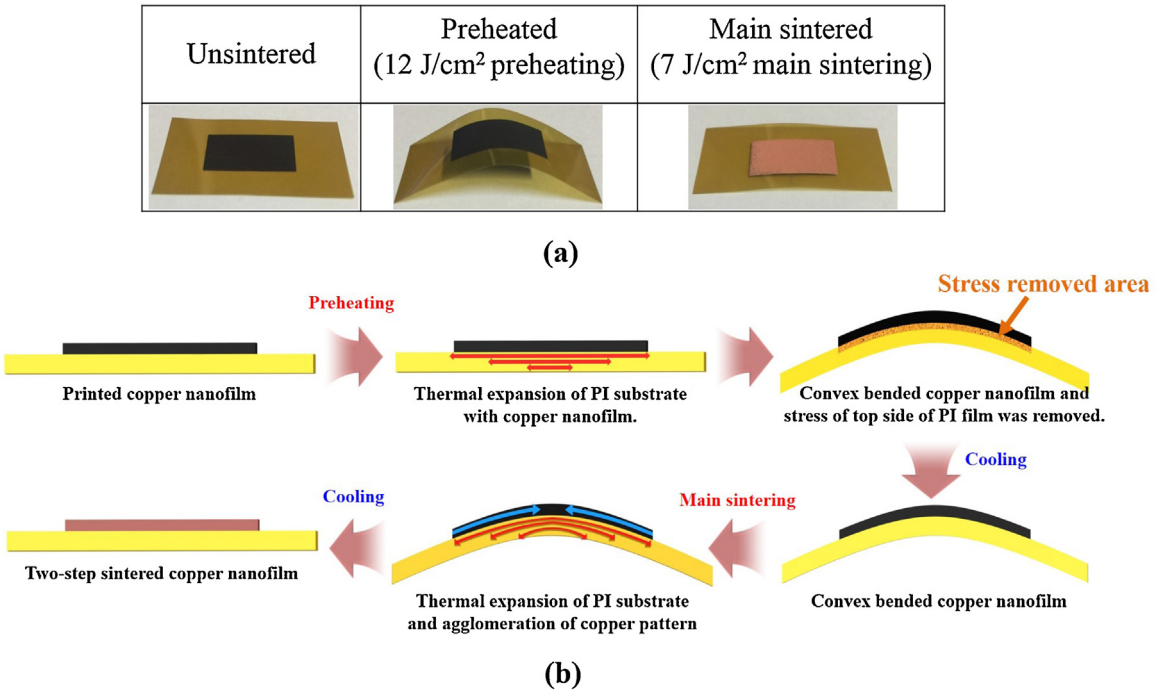

Fig. 13. (a) The optical images and (b) schematic diagrams of substrate warping reduction during two-step flash light sintering process.

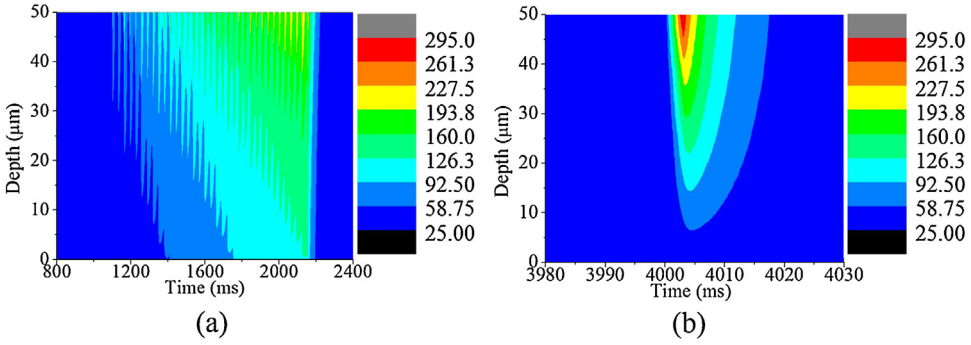

Fig. 14. The temperature changes of PI film in respect to depth and time during two-step flash light sintering process: (a) preheating and (b) main sintering.

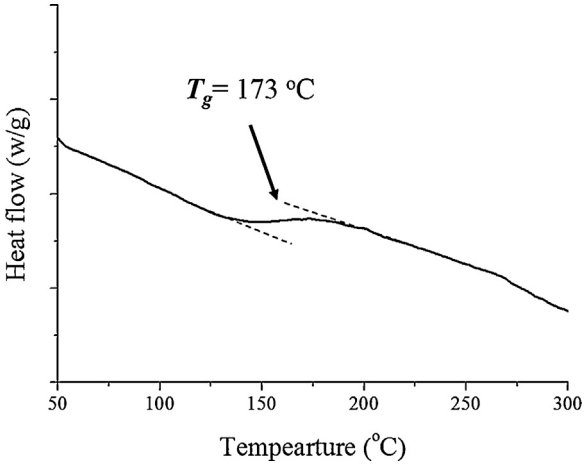

Fig. 15. DSC curve of the PI film used in this work.

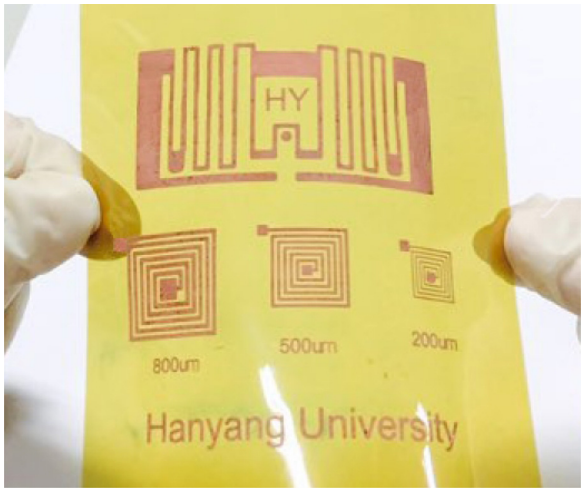

Fig. 16. The two-step sintered copper patterns on PI substrate without any substrate warping.

process, the top surface of the PI substrate adjacent to the copper film was heated rapidly as the temperature of the copper pattern increased up to 230 °C in the preheating process (see Fig. 13(b)). The temperature of the bottom surface of the PI substrate far from the copper film did not increase during the milliseconds duration of the sintering, as the thermal conductivity of the PI film is low. This temperature difference between the top and bottom surfaces of the PI film induce different thermal expansion that generates the convex shape warping as depicted in Fig. 13(b). This result was confirmed by finite element analysis (see Fig. 14(a)). The significant temperature gradient through the depth direction of PI film was observed during preheating process due to its low thermal conductivity. Therefore, these temperature gradients contributed to the convex shape of PI film. Also, in that high temperature, the top of the PI film was softened during preheating process. It is because the glass transition temperature of PI film is about 173 °C from the DSC analysis as shown in Fig. 15 [28]. Hence, the internal stress of top of the PI film was decreased to almost zero due to the glass-transition phenomena beneath the preheated Cu nanoink film, which allows PI film in convex shape after cooling. Then, after the 7 J/cm^2 main sintering energy was applied, the copper pattern and PI substrate also heated up and expanded together, which shrank again when it was cooled down (Figs. Fig. 13(b) and Fig. 14(b)). During this step, the copper pattern's shrinkage compensates for the convex warping of the PI substrate due to its high modulus, while it does not dominate the warping during the shrinkage after the preheating step. Note that after the main sintering step, the copper nanoink film was transformed as a fully sintered metal copper film with a high elastic modulus. the cooling steps after the preheating and main sintering are similar. Major differences between two cooling cases after the preheating and the main sintering, are the materials properties of the Cu films: Unsintered one or fully sintered one. During the cooling after the preheating step, the copper nanoparticles are not sintered at all exhibiting almost no modulus: the gathered copper nanoparticles have almost no modulus in a macroscopic view, thus it does not contribute to the warpage generation and its shape during cooling. Meanwhile, during the cooling after the main sintering, the copper patterns are fully sintered and exhibit the high modulus of the metal Cu film. Therefore, during the cooling, it shrinks compensating the PI warpage in opposite direction, which makes the entire film flat.

Consequently, the preheating improved the electrical conductivity and removed the warping of the copper nanoink film. As a result, the resistivity of the two-step sintered copper nanoink films was 3.81 μΩ cm, which is approximately 2.3 times greater than that of the bulk copper by dividing sintering process into two procedures, reduction and sintering processes, as mentioned above. Also, these findings are corresponding with temperature monitoring, resistance monitoring, FT-IR, and XRD analysis. Therefore, the two-step sintering is determined that copper nanoink film has high conductivity with enhanced crystallization of copper structure, contrary to the one-step sintered case. Using the optimized two-step sintering technique, highly conductive copper nanoink films could be successfully printed and sintered without any warping of the substrate (Fig. 16).

4. Conclusion

In this study, a two-step sintering method was devised to reduce substrate warping and enhance conductivity. The opti-

mized two-step flash light sintering process (12 J/cm^2 preheating followed by 7 J/cm^2 main sintering) sintered the copper pattern on the PI substrate without residual warping and its resistivity was 3.81 μΩ cm, which is approximately 2.3 times of that of bulk copper. Also, the adhesion strength of two-step sintered copper nanoink film has 5B level than that of one-step sintered case is 3B level. The two-step sintering mechanism was analyzed using resistance and temperature monitoring of copper nanoink film, and these results were verified with the simulation result considering heat transfer analysis of copper nanoink film and PI substrate. Also, various characterizations such as SEM image, resistance monitoring, temperature monitoring, FT-IR analysis, and XRD patterns demonstrated that the copper nanoink film was fully sintered and densely agglomerated owing to the splitting sintering process into two-step, reduction and sintering. Therefore, two-step flash light sintering can be widely used for printed electronics.

Acknowledgement

This work was supported by a National Research Foundation of Korea (NRF), funded by the Ministry of Education (No. 2012R1A6A1029029 and 2015R1D1A1A09058418). This work was supported by the Technology Innovation Program (or Industrial Strategic technology development program, 10048913, Development of the cheap nano-ink which is sintered in the air for smart devices funded By the Ministry of Trade, industry & Energy (MI, Korea). Also, this work was supported by the Nano-Convergence Foundation (www.nanotech2020.org) funded by the Ministry of Science, ICT, and Future Planning (MSIP, Korea) and the Ministry of Trade, Industry, and Energy (MOTIE, Korea) [Project Number: R201502510].

References

[1] B.K. Park, D. Kim, S. Jeong, J. Moon, J.S. Kim, Direct writing of copper conductive patterns by ink-jet printing, Thin Solid Films 515 (2007) 7706–7711.
[2] J. Perelaer, A.W. de Laat, C.E. Hendriks, U.S. Schubert, Inkjet-printed silver tracks: low temperature curing and thermal stability investigation, J. Mater. Chem. 18 (2008) 3209–3215.
[3] Q. Cao, H.-s. Kim, N. Pimparkar, J.P. Kulkarni, C. Wang, M. Shim, K. Roy, M.A. Alam, J.A. Rogers, Medium-scale carbon nanotube thin-film integrated circuits on flexible plastic substrates, Nature 454 (2008) 495–500.
[4] A. Kamyshny, J. Steinke, S. Magdassi, Metal-based inkjet inks for printed electronics, Open Appl. Phys. J. 4 (2011).
[5] A. Kamyshny, S. Magdassi, Conductive nanomaterials for printed electronics, Small 10 (2014) 3515–3535.
[6] V. Subramanian, J.M. Fréchet, P.C. Chang, D.C. Huang, J.B. Lee, S.E. Molesa, A.R. Murphy, D.R. Redinger, S.K. Volkman, Progress toward development of all-printed RFID tags: materials, processes, and devices, Proceedings of the IEEE 93 (2005) 1330–1338.
[7] S.M. Bidoki, D. McGorman, D.M. Lewis, M. Clark, G. Horler, R.E. Miles, Inkjet printing of conductive patterns on textile fabrics, AATCC Rev. 5 (2005) 11.
[8] S.K. Volkman, Y. Pei, D. Redinger, S. Yin, V. Subramanian, Ink-jetted silver/copper conductors for printed RFID applications, MRS Proceedings 8 (2004) I7 (Cambridge Univ Press).
[9] R.-Z. Li, A. Hu, T. Zhang, K.D. Oakes, Direct writing on paper of foldable capacitive touch pads with silver nanowire inks, ACS Appl. Mater. Interfaces 6 (2014) 21721–21729.
[10] K. Woo, D. Kim, J.S. Kim, S. Lim, J. Moon, Ink-Jet printing of cu- ag-based highly conductive tracks on a transparent substrate, Langmuir 25 (2008) 429–433.
[11] Y. Lee, J.-r. Choi, K.J. Lee, N.E. Stott, D. Kim, Large-scale synthesis of copper nanoparticles by chemically controlled reduction for applications of inkjet-printed electronics, Nanotechnology 19 (2008) 415604.
[12] J. Perelaer, B.J. de Gans, U.S. Schubert, Ink-jet printing and microwave sintering of conductive silver tracks, Adv. Mater. 18 (2006) 2101–2104.
[13] W.-S. Han, J.-M. Hong, H.-S. Kim, Y.-W. Song, Multi-pulsed white light sintering of printed Cu nanoinks, Nanotechnology 22 (2011) 395705.
[14] H.-J. Hwang, W.-H. Chung, H.-S. Kim, In situ monitoring of flash-light sintering of copper nanoparticle ink for printed electronics, Nanotechnology 23 (2012) 485205.
[15] Y.-J. Kim, C.-H. Ryu, S.-H. Park, H.-S. Kim, The effect of poly (N-vinylpyrrolidone) molecular weight on flash light sintering of copper nanopaste, Thin Solid Films 570 (2014) 114–122.
[16] J. Ryu, H.-S. Kim, H.T. Hahn, Reactive sintering of copper nanoparticles using intense pulsed light for printed electronics, J. Electron. Mater. 40 (2011) 42–50.
[17] S.-J. Joo, H.-J. Hwang, H.-S. Kim, Highly conductive copper nano/microparticles ink via flash light sintering for printed electronics, Nanotechnology 25 (2014) 265601.
[18] R.-Z. Li, A. Hu, D. Bridges, T. Zhang, K.D. Oakes, R. Peng, U. Tumuluri, Z. Wu, Z. Feng, Robust Ag nanoplate ink for flexible electronics packaging, Nanoscale 7 (2015) 7368–7377.
[19] S.-H. Park, W.-H. Chung, H.-S. Kim, Temperature changes of copper nanoparticle ink during flash light sintering, J. Mater. Process. Technol. 214 (2014) 2730–2738.
[20] I.-H. Lai, K.-S. Chou, Effect of titania addition on adhesion of silver colloids to glass substrate, J. Adhes. (2015).
[21] M. Wang, J. Wang, W. Chen, Y. Cui, L. Wang, Effect of preheating and annealing temperatures on quality characteristics of ZnO thin film prepared by sol–gel method, Mater. Chem. Phys. 97 (2006) 219–225.
[22] R. Lesyuk, W. Jillek, Y. Bobitski, B. Kotlyarchuk, Low-energy pulsed laser treatment of silver nanoparticles for interconnects fabrication by ink-jet method, Microelectron. Eng. 88 (2011) 318–321.
[23] O.A. Yeshchenko, I.M. Dmitruk, A.A. Alexeenko, A.M. Dmytruk, Size-dependent melting of spherical copper nanoparticles embedded in a silica matrix, Phys. Rev. B 75 (2007) 085434.
[24] K. Sakurai, T. Maegawa, T. Takahashi, Glass transition temperature of chitosan and miscibility of chitosan/poly(N-vinyl pyrrolidone) blends, Polymer 41 (2000) 7051–7056.
[25] H. Kaczmarek, A. Kamińska, M. Świątek, J. Rabek, Photo-oxidative degradation of some water-soluble polymers in the presence of accelerating agents, Die Angew. Makro Mol. Chem. 261 (1998) 109–121.
[26] S. Horikoshi, N. Serpone, Y. Hisamatsu, H. Hidaka, Photocatalyzed degradation of polymers in aqueous semiconductor suspensions. 3. Photooxidation of a solid polymer: tiO2-blended poly (vinyl chloride) film, Environ. Sci. Technol. 32 (1998) 4010–4016.
[27] H. Gil, A. Echavarria, F. Echeverría, Electrochemical reduction modeling of copper oxides obtained during in situ and ex situ conditions in the presence of acetic acid, Electrochim. Acta 54 (2009) 4676–4681.
[28] Y. -z. Guo, D. -x. Shen, H. -j. Ni, J. -g. Liu, S. -y. Yang, Organosoluble semi-alicyclic polyimides derived from 3,4-dicarboxy-1,2,3,4-tetrahydro-6-tert-butyl-1-naphthalene succinic dianhydride and aromatic diamines: synthesis, characterization and thermal degradation investigation, Prog. Org. Coat. 76 (2013) 768–777.